Computation of the radiation force exerted by the acoustic tweezers using pressure field measurements

Dan Zhao, Jean-Louis Thomas, R. Marchiano

Computation of the radiation force exerted by an acoustic tweezers using pressure field measurements

Zhao Dan,[1,2] Jean-Louis Thomas,[1] and Régis Marchiano[2]

[1)] *Sorbonne Université, CNRS, Institut des NanoSciences de Paris, INSP, F-75005 Paris, France*

[2] *Sorbonne Université, CNRS, Institut Jean Le Rond d'Alembert, ∂' Alembert, F-75005 Paris, France*

Acoustic tweezers allow to manipulate small objects like elastic spheres with a force generated by the radiation pressure which arises from the nonlinear interaction between the incident and scattered waves by the object. The accurate control of the object by acoustic tweezers requires the study of the components of the three-dimensional force.If the physical properties of the elastic sphere are known, then the 3D components of the force can be calculated thanks to a decomposition of the incident acoustic field in the spherical functions basis. In this work, we propose to evaluatethe expansion coefficients. Three methods are used and compared. The first one consists in measuring the acoustic field on a spherical surface centered on the theoretical position of the object and to calculate the spherical functions decomposition by Lebedev quadratures. The second method is based on the measurement of the acoustic field at random points in a spherical volume and on the resolution of the inverse problem by a sparse method called the orthogonal matching pursuit. In the third method, the incident beam is measured on a transverse plane, decomposed into a sum of plane waves and then the expansion coefficients are calculated. The results of the three methods will be presented and compared.

I. INTRODUCTION

Acoustic tweezers like optical and magnetic tweezers are used for 3D manipulation of small objects such as cells and molecules. These micro manipulators are in a strong demand in the field of biophysics. Among these tweezers, optical tweezers[1–3] have been developed first and demonstrated their precision and trap capabilities. However, the high intensity at the focus of optical tweezers can lead to photo-damage and heating of the target object, especially in vivo samples. Magnetic tweezers are not limited by photo-damage and are widely used in the biology field especially for manipulation and analyses of DNA and RNA[23,32]. The main limitation of magnetic tweezers is the limited range of constant-force that can be exerted due to their low trap stiffness. Moreover, applying large force requires high-current electromagnets which would cause heating or produce non constant-force. The radiation force is proportional to the field intensity divided by the speed of propagation. As the velocity of light is 5 orders of magnitude larger than sound speed, acoustic tweezers are able to afford large forces with much smaller intensity than optical tweezers and are a solution for the heating issue. This advantage enables a wide range of applications of acoustic tweezers in various domains such as materials science, study of biophysical properties of cells and molecules, micro-rheology, biophysical characterization of DNA, etc.

Different kinds of acoustic traps exist. Most of them are based on standing waves either in the bulk[35] or propagating at the surface of a solid substrate[13,14]. In these schemes, all pressure nodes (or anti-nodes depending on the object density and compressibility) act as potential traps. On the contrary, optical tweezers are selective traps with a single position of equilibrium. Radial selectivity was achieved by Wu[34] using two counterpropagating focused ultrasonic beams. Single beam acoustic tweezers are characterized by the ability to pick up, trap and manipulate a single small elastic particles in three dimensions[4,5,7,9] as its optical counterpart. For all the possible applications, the calibration of the force provided by acoustic tweezers is of importance, especially for micro-rheology studies. The optical and magnetic tweezers' forces calibration is achieved mainly by two methods: the first one consists in studying the Brownian motion of trapped objects with sizes comparable to the wavelength, then the force is determined from Hooke's law[12,24]; the second one is to use the viscous drag force generated by a controlled fluid flow[25].

Nonetheless, the first method is not applicable for acoustic tweezers since the wavelength and the object can be much larger and the Brownian motion disappears at these scales. As for the second method, the fluid drag forces are also used to calibrate the acoustic trapping force[22], but difficulties arise for single beam acoustic tweezers due to the Magnus effect[16] caused by the rotation of bead in an acoustic vortex beam[8]. Previously, the three dimensional force exerted on a spherical particle was modeled using the incident beam expansion on spherical functions. This model depends on the expansion coefficients, A_n^m, dubbed beam shape coefficients (BSC), and the scattering coefficients of the particle, R_n[6].

In this article, we are interested in characterizing the radiation pressure exerted by acoustic tweezers on a spherical particle using this model. Thus, this is not a direct measurement of the force. The acoustic field is measured with a calibrated hydrophone and then the force is deduced. Section II is a short reminder of the model focused on the equations needed to calculate the radiation pressure exerted on an elastic sphere. To obtain the BSC of the incident pressure field, three methods are numerically investigated in section III: Lebedev quadrature, inverse problem regularization by sparsity and angular spectrum method (ASM). In section IV, a focused Gaussian beam and a focused acoustic vortex are synthesized and measured. The BSC are recovered by applying the three methods. Then, the acoustic field is reconstructed and compared with measurements and finally the radiation pressure is determined by the three methods.

II. THEORETICAL BACKGROUND: RADIATION PRESSURE

Let us consider a 3D Cartesian system of coordinates (x, y, z). The three components of radiation pressure exerted on an arbitrarily located elastic sphere in a perfect fluid by an arbitrarily incident beam are[6]:

$$F_x = -\frac{\langle V\rangle}{k_0^2}\sum_{n=0}^{\infty}\sum_{|m|<n}\Im(Q_n^{-m}A_n^{m*}A_{n+1}^{m-1}C_n + Q_n^m A_n^m A_{n+1}^{m+1*}C_n^*), \tag{1}$$

$$F_y = +\frac{\langle V\rangle}{k_0^2}\sum_{n=0}^{\infty}\sum_{|m|<n}\Re(Q_n^{-m}A_n^{m*}A_{n+1}^{m-1}C_n + Q_n^m A_n^m A_{n+1}^{m+1*}C_n^*), \tag{2}$$

$$F_z = +2\frac{\langle V\rangle}{k_0^2}\sum_{n=0}^{\infty}\sum_{|m|<n}\Im(G_n^m A_n^{m*}A_{n+1}^{m}C_n). \tag{3}$$

With :

$$V = p_0^2/(4\rho_0 c_0^2),$$

$$C_n = R_n^* + R_{n+1} + 2R_n^* R_{n+1},$$

$$Q_n^m = \sqrt{(n+m+1)(n+m+2)}/\sqrt{(2n+1)(2n+3)},$$

$$G_n^m = \sqrt{(n+m+1)(n-m+1)}/\sqrt{(2n+1)(2n+3)}.$$

$p_a(x, y, z, t)$ is the linear component of the acoustic pressure, its time average is zero. ρ_0 and c_0 are respectively the fluid density and speed of sound at rest. Coefficients A_n^m are the coefficients of the expansion into spherical functions:

$$p_a(r, \theta, \varphi, t) = p_0 \sum_{n=0}^{\infty} \sum_{|m|<n} A_n^m j_n(kr) Y_n^m(\theta, \varphi) exp(-i\omega t) \tag{4}$$

where the spherical harmonics are defined by:

$$\begin{aligned} Y_n^m(\theta, \varphi) &= \sqrt{\frac{(2n+1)}{4\pi} \frac{(n-m)!}{(n+m)!}} P_n^m(\cos\theta) e^{im\varphi} \\ &= N_n^m P_n^m(\cos\theta) e^{im\varphi} \end{aligned} \tag{5}$$

with (r, θ, φ) the spherical coordinates linked to the Cartesian coordinates by $x = r\sin\theta\cos\varphi$, $y = r\sin\theta\sin\varphi$ and $z = r\cos\theta$. j_n designates the spherical Bessel function, $P_n^m(\cos(\theta))$ are the Legendre polynomials and k is the wave number. The azimuthal number m and the radial degree n satisfy $|m| \leq n$.

From the theoretical expressions of the radiation pressure, two sets of coefficients are required to determine the forces:

- Scattering coefficients: R_n

- Incident BSC: A_n^m

The scattering coefficients R_n for an arbitrary incident beam are known and depend only on the physical characteristics of the object and propagation medium[6]. Therefore, our problem of determining the radiation forces can be solved by searching the incident BSC A_n^m. These coefficients are known analytically for several beams (plane wave, Bessel beam, vortex beam). Nevertheless, in real applications the pressure field is sampled in time and in space on a finite set of points and make the determination of BSC a challenge. In the following part, three different methods for calculating these coefficients are investigated.

III. CALCULATION OF BEAM SHAPE COEFFICIENT A_n^m FROM THE PRESSURE FIELD

For each method, the determination of the BSC is tested on the same incident field: a focused vortex beam of topological charge $m' = 1$. This beam is very important because, it is the keystone to create acoustic tweezers[4,5,7,28]. As this paper proposes to address the problem of the characterisation of the radiation force and especially the one exerted by acoustic tweezers, it is reasonable to validate the methodology on a field as close as possible to the final target. The BSC for a focused vortex beam are[5]:

$$A_n^m = \delta_{m,m'} 4\pi (kr_0)^2 h_n^{(1)}(kr_0) \int_{\pi-\alpha_0}^{\pi} P_n^{m'}(cos\theta') N_n^{m'} d\theta'. \tag{6}$$

with $\delta_{m,m'}$ the Kronecker delta, $h_n^{(1)}$ the spherical Hankel function of first kind, m' the topological charge of the vortex and α_0, a_0, r_0 are respectively the aperture half angle, the radius of the transducer and the focal distance as illustrated on top of Fig. 1. In this paper, we use the expression of normalized spherical harmonics with a factor N_n^m (see Eq. 5), hence A_n^m are different from previous works[6],[5].

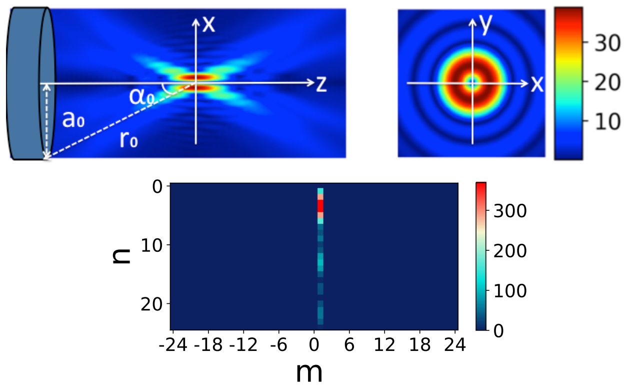

FIG. 1. (Top) Modulus of the complex pressure field at frequency corresponding to a wavelength of $1.25mm$ in water, and (bottom) BSC, for a focused vortex with topological charge $m' = 1$ the spherical basis is centered at the focus of the incident beam (color online)

Using Eq. 4, the pressure field can be computed anywhere. Fig. 1 shows the pressure field for a focused vortex beam of charge $m' = 1$ (top row), and the BSC (bottom). We selected the case of water, $c_0 = 1500m \cdot s^{-1}$, as propagating medium and a frequency of $1.2MHz$. The wavelength is $\lambda = 1.25mm$. The pressure field has a zero amplitude along the axis of propagation. This is a common feature associated with vortex beam[19,26]. The focusing is sharp because the aperture of the transducer is $110mm(88\lambda)$, $75mm(60\lambda)$ away from the focus (corresponding to an aperture half angle equal to $\alpha_0 = 43^o$). As expected the BSC are restricted to the column $m = 1$ with a non intuitive variation in function of the radial degree. We assessed numerically the error on the radiation force, Eq. 1-3 by decreasing the truncation order. Thereafter, all series are truncated at $n \leq N = 25$ and the error on the force is 0.001.

A. Lebedev Quadrature

The first method is based on the orthogonality of the spherical harmonics: $< Y_n^m, Y_{n'}^{m'} >= \delta_{n,n'}\delta_{m,m'}$ where the scalar product on the sphere is defined by $< f(\theta,\varphi), g(\theta,\varphi) >= \int\int f(\theta,\varphi)g(\theta,\varphi)\sin\theta d\theta d\varphi$. By applying this property, BSC A_n^m can be expressed by integrals over a spherical surface:

$$\begin{aligned} A_n^m &= \frac{1}{p_0 j_n(kr)} < p, Y_n^m > \\ &= \frac{1}{p_0 j_n(kr)} \int_\theta \int_\varphi p(\theta,\varphi) Y_n^{m*}(\theta,\varphi)\sin\theta d\theta d\varphi. \end{aligned} \tag{7}$$

The integrals in Eq. 7 are computed by numerical integration. Using a numerical quadrature to perform this integration in the context of acoustic radiation force or torque have already been investigated[17,18]. In these previous works, the sphere was sampled with a very fine grid incompatible with actual measurements of the pressure fields and there was no noise. Different quadrature rules have been tested: Legendre-Gauss quadrature, Chebyshev quadrature[10] and Lebedev quadrature. Among these quadratures, the Lebedev quadrature[31] gives the best precision for a given number of points and only that quadrature is used here[21]. The number, position and the weight of Lebedev grids defined on an unit sphere ((x_i, y_i, z_i) and weights w_i) have been derived by Sobolev[31]. Therefore, measuring the pressure field at the Lebedev points (see Fig. 2 to visualize their positions) and using this quadrature give the BSC A_n^m.

$$A_n^m = \frac{1}{p_0 j_n(kr)} \sum_{i=0}^{I-1} p(\theta_i, \varphi_i) Y_n^{m*}(\theta_i, \varphi_i) w_i. \quad (8)$$

Lebedev quadrature has optimal efficiency, i.e. the number of points required, $I = (\mathcal{N}+1)^2/3$, is the smallest, where $\mathcal{N}$ is the highest order of the polynomials integrated on the sphere. Moreover, the distance between the Lebedev points is roughly constant. This feature is very interesting since it provides an optimal sampling of the sphere in regards with the finite size of an hydrophone and thus it optimizes the signal-to-noise-ratio (SNR) The integrand is the product of spherical harmonics, Eq. 4, 7. If the series is truncated at $n \leq N$, the integrand is a polynomial of order smaller than $2N$ and hence $\mathcal{N} = 2N$. For our case, $N = 25$ and this yields $I = 867$. It must be noted that the number of Lebedev points is not arbitrary. Here, we use $I = 974$ Lebedev points on a sphere with radius $7mm(5.6\lambda)$. This choice amendellows to perfectly retrieve the high order modes (here up until $n = 25$) as shown in Fig. 2, the BSC obtained by the Lebedev quadrature for a focused vortex beam. Of course, this previous estimation does not take into account the noise in the measurements. It is known that the determination of the BSC are prone to errors in the presence of noise[29]. To assess the robustness of the method in presence of noise, we proceed in three steps. First, the BSC of Eq. 6, named thereafter $A_{n_{th}}^m$, are computed and the corresponding pressure field calculated with Eq. 4 on the Lebedev grid and in the focal plane to determine the maximum pressure. Second, a noise with a uniform distribution in an interval of amplitude 5% of this maximum pressure is added to the pressure field calculated on the Lebedev grid. Third, the BSC of this noisy pressure field, noted A_n^m, are estimated with Eq. 8 and shown on Fig. 2. In Fig. 2, the lines where the BSC are very different from the original ones correspond to the values closest to zero for the Bessel function (Fig. 3). Indeed, since the scalar product with spherical harmonics is a linear operation, the result is the scalar product with the ideal pressure fields plus the scalar product with the noise. Hence the error is proportional to $1/j_n(kr)$. On Fig. 3, we can observe a first oscillating part up to $n = 35$ followed by a fast decrease converging to 0. We selected a sphere radius large enough, $7mm(5.6\lambda)$, so that the truncature order $N = 25$ is located in the oscillating part.

To assess the numerical performance of the method, we compute the relative error:

$$err = \frac{1}{(N+1)^2} \sum_{n=0}^{N} \sum_{m=-n}^{m=n} \frac{|A_n^m - A_{n_{th}}^m|}{max(|A_{n_{th}}^m|)} \tag{9}$$

$(N+1)^2$ is the total number of BSC A_n^m of order $n \leq N$. Here the relative error is 0.061.

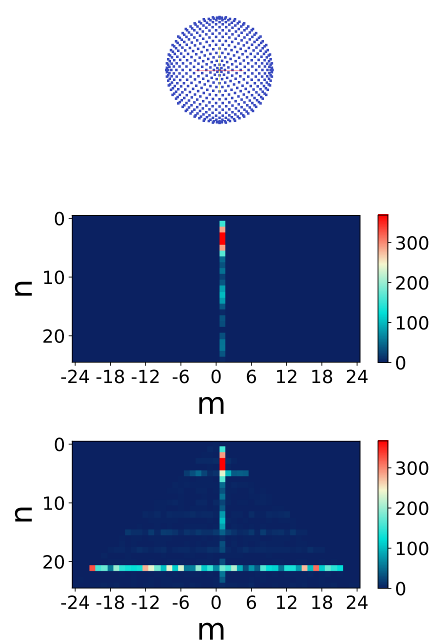

FIG. 2. (Top) points on a Lebedev sphere, and (Middle) reconstructed BSC for an incident focused vortex beam without noise and (Bottom) with 5% noise. (color online)

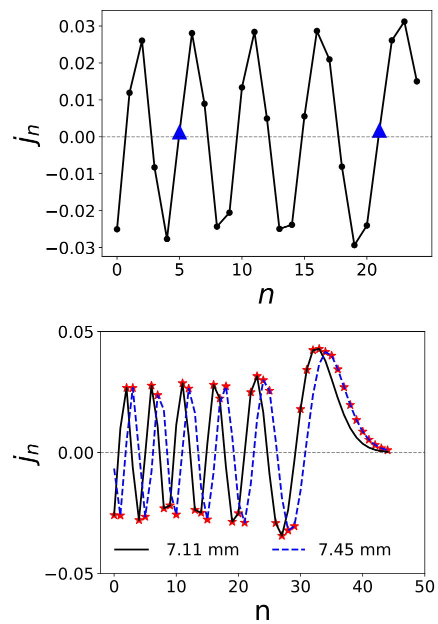

FIG. 3. (Top) Amplitude of the spherical Bessel $j_n(kr)$ function for a radius $r = 7mm(5.6\lambda)$ (the blue triangles show the values close to zero) and (Bottom) for two different radii $r_1 = 7.11mm(5.7\lambda)$ and $r_2 = 7.45(6\lambda)$ (the red points show the maximum values between $|j_n(kr_1)|$ and $|j_n(kr_2)|$ for each order n). The frequency is $f_0 = 1.2MHz$. (color online)

An upgrade in order to mitigate the detrimental effect of noise is to use a double layer Lebedev sphere[29]. The idea is to use two spheres with different radii and to apply the Lebedev quadrature, for a given ordrer n, to the sphere for which the Bessel function has the greatest absolute value. Using the asymptotic behavior of Bessel function for large x compared to n, $j_n(x) \approx \cos(x - \pi/2)/x$, in Fig. 3, we selected the radius of the second sphere such that $j_n(x') \approx \sin(x' - \pi/2)/x'$ to optimize the estimation, this leads to $r_1 = 7.11\ mm(5.7\lambda)$ and $r_2 = 7.45\ mm(6\lambda)$. The red stars indicate the chosen value between the two Bessel functions to compute the BSC of order n. The double layer Lebedev sphere grids are presented in Fig. 4. For each sphere, 974 Lebedev points are used. Fig. 4 shows the

BSC obtained with this method. They are close to the original ones (Fig. 1) and the relative error decreases from 0.06 to 0.015. Nevertheless, one can see that the BSC for $m \neq 1$ are not strictly equal to zero and thus a weak error remains on the estimated BSC.

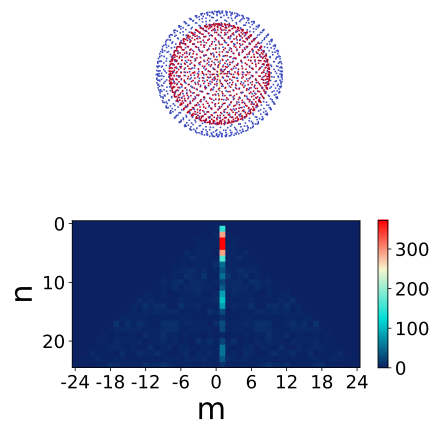

FIG. 4. (Top) measurement points of a double layer Lebedev sphere, (Bottom) reconstructed BSC for an incident focused vortex beam with 5% noise by the double layer Lebedev quadrature method. (color online)

B. Regularization of the inverse problem by a sparse method

Instead of solving Eq. 7 with its discretized version Eq. 8, another strategy consists in solving Eq. 4 whose discretized counterpart can be reformulated under a matrix/vector form:

$$\underline{P} = \underline{\underline{M}}\,\underline{A} + \underline{\epsilon}. \tag{10}$$

with vector $\underline{P}$ whose components are the Fourier transform of the pressure field at frequency f_0 at points of discretization $(x_i, y_i, z_i) : \hat{p}(x_i, y_i, z_i, f_0)$ of length I, vector $\underline{A}$ whose components are the BSC $A_l = A_n^m$ with $l = n(n+1) + m$ of length $L = (N+1)^2$, the matrix $\underline{\underline{M}}$ whose elements are $(j_n(kr_i)Y_n^m(\theta_i, \varphi_i))$ with $(r_i, \theta_i, \varphi_i)$ the points (x_i, y_i, z_i) written in spherical coordinates of size $(I \times L)$and vector $\underline{\epsilon}$ the additive noise on points (x_i, y_i, z_i). To compare this method with the double layer Lebedev sphere quadrature, we set the same number of points: 1948 dispersed in a spherical volume of identical radius $r = 7.11mm(5.7\lambda)$. As previously, the truncature order is set to 25. At this stage the points distribution is free and this can be used to avoid an ill-conditioned matrix. Then, the best choice is a set of random points distributed in a spherical volume as illustrated on Fig. 5.

Because of the noise, the matrix $\underline{\underline{M}}$ is always full rank, the direct inversion is then always possible but unstable in regard of a small change in the noise. This ill-posed problem required regularization to get a meaningful solution. As can be seen on Fig. 1 for a focused vortex beam, a large number of BSC are null. So, vector $\underline{A}$ is sparse. This *a priori* can be used to regularize the inversion:

$$\underline{\tilde{A}} = \mathrm{argmin}\, ||\underline{A}||_0 \text{ such as } \underline{P} = \underline{\underline{M}}\,\underline{A} \tag{11}$$

With this formulation, vector $\underline{\tilde{A}}$ is searched with a particular constraint: it must contain a minimum of non-zero terms.

To solve Eq. 11, we choose to use Orthogonal Matching Pursuit algorithm (OMP)[11]. This algorithm is iterative. For each iteration, the component of $\underline{\underline{M}}$ with the highest inner product with the remaining part of vector $\underline{P}$ is selected. Then its contribution is subtracted and the iterations continue on the residue. This procedure stops when the iteration reaches the number of non-zero elements of the BSC (25 in our case) or when the residual reaches a limit.

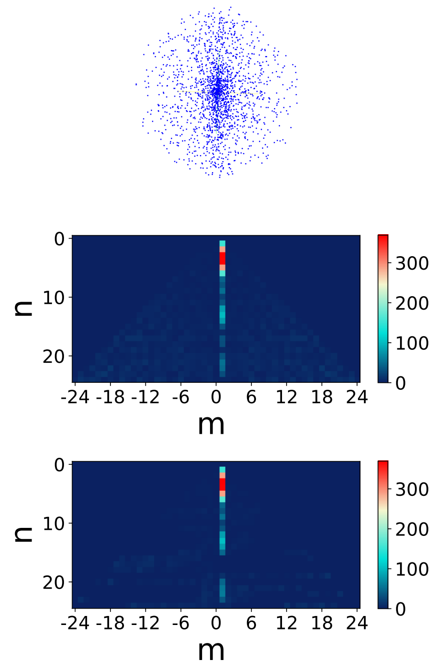

FIG. 5. (Top) randomly distributed measurement points in a sphere, and (Middle) reconstructed BSC for an incident focused vortex beam with 5% noise by the OMP method and (Bottom) block-OMP method. (color online)

With the OMP method, we should be able to recover the BSC on the column $m = 1$ with 25 iterations. However, tests for a vortex beam have shown the inefficiency of this stopping criterion. Thus, the stopping criterion of the OMP procedure will be the residual limit (lower than 0.001). Fig. 5 shows the BSC obtained with the OMP algorithm for the same noisy pressure field as before.There is a very good agreement with the original set of BSC even if some BSC laying outside the column $m = 1$ are not exactly set to zero. Here, the relative error is 0.0141 close to the 0.015 obtained with the Lebedev method. A drawback is the number of iteration required, the computation can be very long. A method to improve this is the Block version of OMP. It's the same procedure but with the matrix $\underline{\underline{M}}$ in a block version[15]. Fig. 5 shows the BSC obtained by applying the Block-OMP method, the matrix $\underline{\underline{M}}$ is divided into blocks of $(N \times 10)$, and the iteration number is 35 only. An unexpected result is that the relative error is then twice better : 0.006

C. Angular spectrum method (ASM)

A third approach is to use a transformation from angular spectrum to spherical harmonics.[30]. The Fourier transform of the pressure in plane z can be seen as a superposition of plane waves:

$$\begin{aligned}\hat{p}(x,y,z,\omega) =& \\ \frac{1}{4\pi^2}\int\int_{k_x^2+k_y^2\leq k^2} & S(k_x,k_y)e^{ik_x x+ik_y y+i\sqrt{k^2-k_x^2-k_y^2}z}dk_x dk_y,\end{aligned} \tag{12}$$

where the angular spectrum $S(k_x,k_y)$ is the 2D spatial Fourier transform of the pressure in plane $z=0$:

$$S(k_x,k_y) = \int_{-\infty}^{+\infty}\int_{-\infty}^{+\infty}\hat{p}(x,y,z=0,\omega)e^{-i(k_x x+k_y y)}dxdy, \tag{13}$$

According to[30], the pressure field can be rewritten:

$$\begin{aligned}\hat{p}(x,y,z,\omega) =& \frac{1}{\pi}\sum_{n=0}^{\infty} i^n j_n(kr)\sum_{m=-n}^{n} Y_{nm}(\theta,\varphi) \\ & \int\int_{k_x^2+k_y^2\leq k^2} S(k_x,k_y)Y_{nm}^*(\theta_k,\varphi_k)dk_x dk_y,\end{aligned} \tag{14}$$

with: $k_x = k\sin(\theta_k)\cos(\varphi_k)$ $k_y = k\sin(\theta_k)\sin(\varphi_k)$ and $k_z = k\cos(\theta_k)$. The comparison of Eq. 4 and Eq. 14 shows that the A_n^m can be written as:

$$A_n^m = \frac{i^n}{\pi}\int\int_{k_x^2+k_y^2\leq k^2} S(k_x,k_y)Y_{nm}^*(\theta_k,\varphi_k)dk_x dk_y. \tag{15}$$

The noisy pressure field is simulated here on a square grid of dimension $7mm \times 7mm (5.6\lambda \times 5.6\lambda)$ regularly sampled with a total of 2500 points. Note that the mesh grids of ASM should be very fine otherwise errors of integration in Eq. 15 arise.The square grid is located at the focal distance $(x, y, z = 0)$. This field is Fourier transformed (Eq. 13) with a discrete Fourier transform (DFT). The sampling after a DFT can be refined by zero-padding for instance. We performed a polynomial interpolation instead. Indeed, knowing the polynomial coefficients, numerical integration of Eq. 15 can be achieved with a variable step method to increase accuracy.

Fig. 6 shows the BSC obtained with the ASM method The agreement with the original BSC is quite good especially for column $m = 1$. Nevertheless, other columns contain non null BSC with a relative important amplitude. The relative error is 0.014.

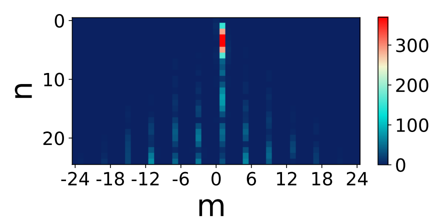

FIG. 6. Computation of the BSC by angular spectrum decomposition. (color online)

Therefore, all methods except the Lebedev quadrature on a single sphere allow to retrieve the BSC for a focused vortex beam with a good confidence even in presence of noise. The results are synthesized in Tab. I.

D. Estimation of the radiation pressure by the three methods

To assess the efficiency of each method, we calculate the radiation forces exerted on a polystyrene sphere of radius $r = 0.1\lambda$ using equations 1, 2, 3. These forces are then decom-

Methods	Relative Error
Lebedev quadrature (Single sphere)	0.061
Double layer Lebedev quadrature	0.015
OMP	0.014
Block - OMP	0.006
ASM	0.014

TABLE I. Relative error for three methods

posed into three components: radial, azimuthal and axial forces (F_ρ, F_ϕ, F_z) in a cylindrical basis (ρ, ϕ, z). On the left of Fig. 7, the forces are calculated by using all the BSC obtained by the three methods, while on the right of Fig. 7, the forces are computed with A_n^1 only. All methods yield accurate estimations of the radial force. On the contrary, the azimuthal force, F_ϕ, has a much weaker amplitude and all methods give poor estimates. Nevertheless, OMP method roughly recovers the original shape of the force. These differences originate from the estimated BSC with finite value outside column $m = 1$. It is shown in Fig. 7 that after filtering out these BSC, all methods recover perfectly the theoretical force. In the case of the axial force, F_z, both OMP and the ASM turn out to provide good estimations while again, the Lebedev method is less efficient and leads to fast oscillations around the expected curve. However, these errors can not be reduced by filtering BSC outside $m = 1$. We may assume that the error is hidden in column $m = 1$.

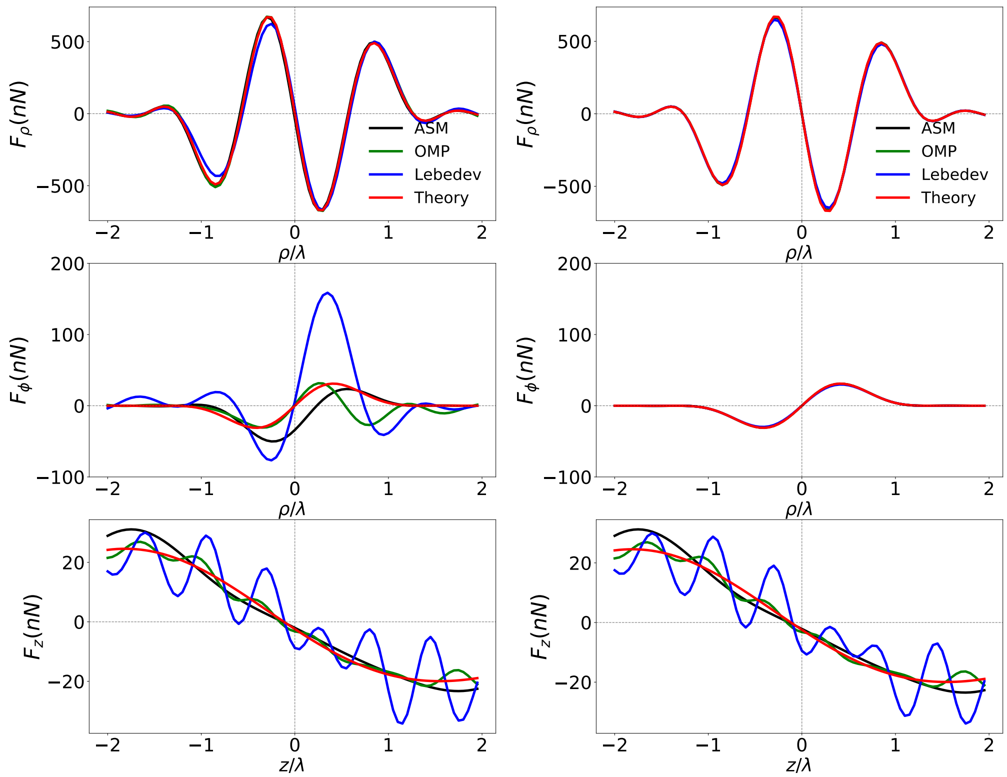

FIG. 7. (Left) radiation force exerted on a polystyrene sphere of radius $r = 0.1\lambda$ with all the BSC, and (Right) with only BSC on column $m = 1$. (color online)

The oscillations on the axial force calculated by Lebedev method are periodical, similar to those caused by a standing wave. Moreover, we know that the radiation pressure due to a standing wave is much stronger than the one due to a progressive wave[20]. Any error on the estimated BSC in this regard should lead to large discrepancies on the force estimation. In order to investigate this assumption, a weak amplitude wave propagating in the opposite direction is superposed to the incident wave. The BSC of the counter propagating wave can be computed as follow. The symmetry $z \to -z$ transforms $\cos(\theta)$ into $\cos(\pi - \theta) = -\cos(\theta)$. Then, considering that the associated Legendre functions $P_n^m(\cos(\theta))$ satisfy the relation :

$$P_n^m(-x) = (-1)^{(n+m)} P_n^m(x). \tag{16}$$

and Eq. 4, 5, the BSC of the wave propagating in the opposite direction can be computed by multiplying the BSC by $(-1)^{(n+m)}$. Taking into account the mean relative error on the estimated BSC 0.006 for block OMP, we fixed the amplitude of this weak counterpropagating wave at 0.005 so that the new BSC are $(1 + 0.005(-1)^{(n+m)})A^m_{n_{th}}$. On Fig. 8 is plotted the axial force for the progressive wave only and with the counterprogating wave superposed. Comparing with Fig. 7, oscillations with the same periodicity but weaker amplitudes are obtained.

There remains to explain why the Lebedev method is more sensitive to the noise than the

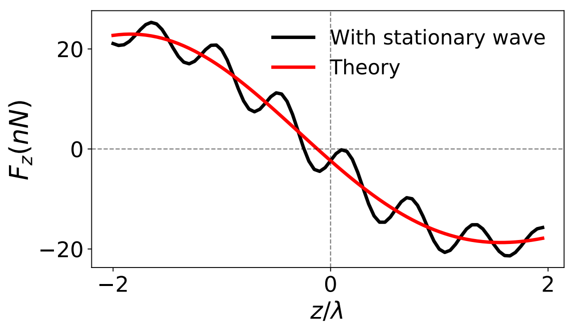

FIG. 8. Axial force exerted on a polystyrene sphere of radius $r = 0.1\lambda$ with theoretical BSC A^m_n (black) and theoretical BSC with a counter propagating wave with 0.5% amplitude (red). (color online)

other two methods. In our simulation, the random noise amplitude is evenly distributed between -5% and 5% of the maximum pressure of the incident beam in all three cases. However for Lebedev quadrature, the pressure field is sampled at the surfaces of two spheres with radius $r = 7.11mm(5.7\lambda)$ and $r = 7.45mm(6\lambda)$ where the wave is either yet converging, $z < 0$, or diverging, $z > 0$. Since the wave is sharply focused, on these spheres its amplitude and hence the SNR is $10dB$ lower.On the contrary, the set of points used either inside a spherical volume (OMP) or on a focal plane (ASM) contains locations where the pressure amplitude is maximum. By calculating the SNR at a measurement point where the signal is the maximum for each method, we obtain the results of $22.5dB$, $32.2dB$ and $32.5dB$ for the Lebedev quadrature, OMP and ASM respectively. To confirm the role played by the SNR, the OMP method is now applied in conditions similar to the ones used for Lebedev quadrature. The pressure field is sampled on a set of points randomly distributed on a spherical surface of $r = 7mm(5.6\lambda)$. The axial force obtained by the two methods are now similar with oscillating errors of about the same period and amplitude. Besides, if we increase the radius to $10mm(8\lambda)$, the fluctuations become stronger as expected since the SNR is even more degraded.

To compare the numerical estimation of the forces by different methods (with all the BSC

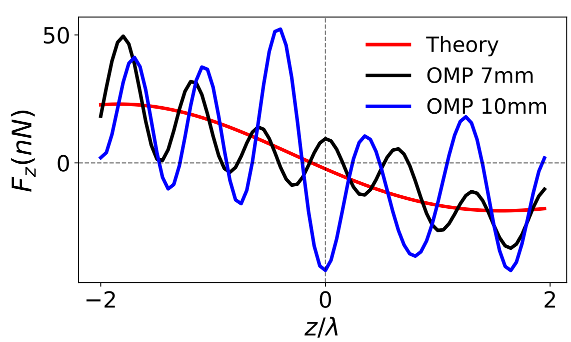

FIG. 9. Axial force exerted on a polystyrene sphere of radius $r = 0.1\lambda$ with BSC computed by OMP method on two spherical surfaces (black and blue) and the theoretical force (red). (color online)

A_n^m), the relative errors between the force calculated with the A_n^m, F, in the presence of noise and the force computed with the $A^m_{n_{th}}$, F_{th}, are then calculated :

$$err_{force} = \frac{1}{K}\frac{\sum_0^K |F - F_{th}|}{max|F_{th}|} \tag{17}$$

K is the total number of positions where the forces are estimated. The results are presented in Tab. II. We can conclude that both the OMP and angular spectrum are effective methods for estimating the radiation force from pressure field measurements with very low relative error as presented in Tab. II. The task is nevertheless difficult since small errors potentially result in spurious standing waves and the radiation pressure exerted by standing waves is much stronger than for progressive waves.

Relative error	Lebedev	OMP	ASM
F_ρ	0.036	0.012	0.018
F_ϕ	0.87	0.23	0.22
F_z	0.29	0.056	0.096

TABLE II. Relative error of the forces for three methods

IV. EXPERIMENTAL MEASUREMENTS

In this section, the three methods are applied on experimental data. A focused Gaussian beam, with charge $m' = 0$, and a focused vortex beam with charge $m' = 1$ have been synthesized using a large antenna made of 120 piezoelectric transducersdistributed on a hexagonal pattern on a concave surface with a radius of curvature of $45cm$. The array aperture is $11cm(88\lambda)$. An acoustic lens is used to reduce this focal to $7.5cm(56\lambda)$. With the lens, the half-angle, α_0, is comparable to the simulated cases. The pressure field is synthesized by selecting the electric signals fed to each transducers by a multichannel electronics made of 120 arbitrary signals generators. These signals are calculated using the inverse filter technique[26,27,33]. The set-up and procedure are identical to the ones used in previous work[7]. The incident sound beam was then measured by a calibrated needle hydrophone of $0.2mm(0.2\lambda)$ diameter (Precision Acoustics Ltd, UK) on three different grids corresponding to the different algorithms presented in the previous section. The measurement grids are all centered on the focal point of the vortex beam. For each location of the hydrophone, an ultrasound burst of 10 cycles is repeated 128 times and the records are averaged to increase the SNR. The experimental SNR is $20dB$ lower than the SNR in the previous section.After these measurements on the different grids, we apply the three methods described in section II to estimate the BSC. The obtained BSC completely describe the field, Eq. 4. We measured the acoustic pressure on the transverse plane (xy) (on the ASM grid) and the vertical plane (xz) (on a rectangular grid of dimension $7mm \times 20mm$ $(5.6\lambda \times 16\lambda)$ with steps of $0.4mm \times 0.3mm$ $(0.3\lambda \times 0.2\lambda)$). A DFT is then used to get the measured pressure in the Fourier domain and then extract the modulus at $1.2MHz$. Fig 10 displays the computed and measured modulus of the pressure field at this frequency. The reconstructed fields computed with the three different methods are in very good agreement with the direct measurements.On the lateral, (xy), plane. The main lobe is perfectly recovered and in the case of the vortex beam the small anisotropy on the bright ring is accurately estimated. The secondary ring of high pressure modulus characteristic of diffraction by a truncated aperture, i.e. the array of transducers, is also efficiently estimated. Compared to simulated

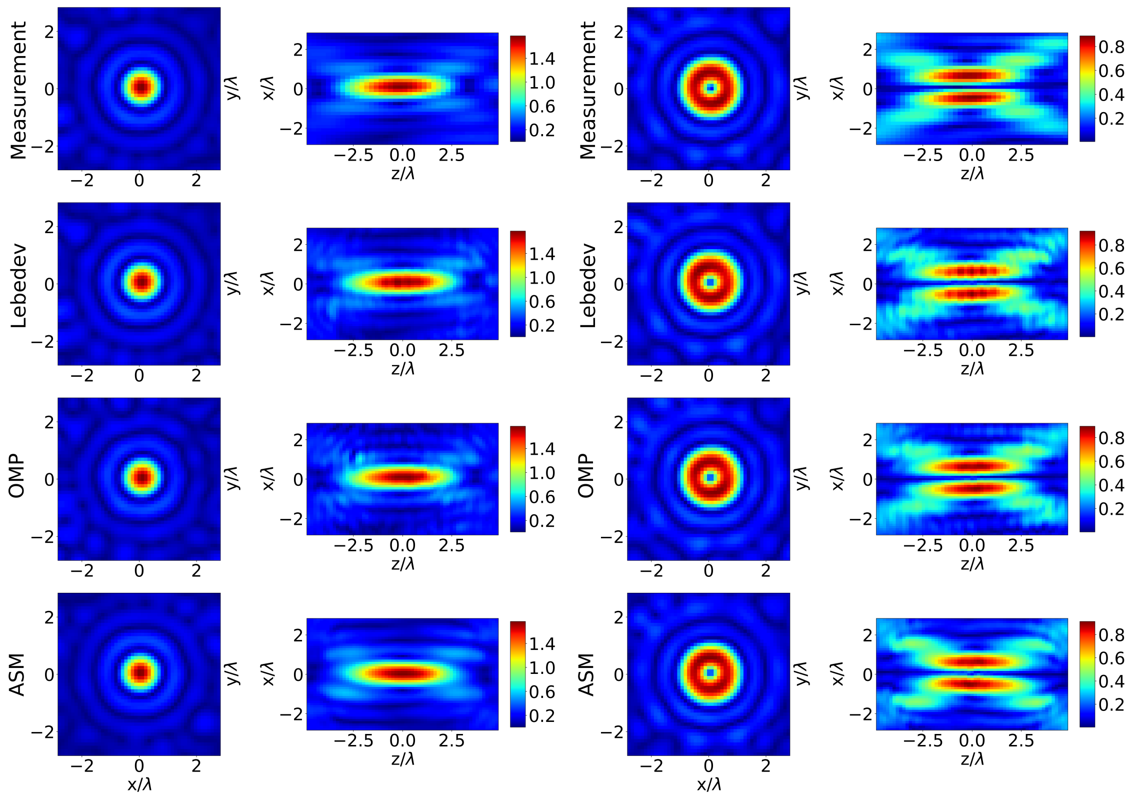

FIG. 10. Reconstruction of the incident beam in Fourier domain, (pressure modulus is shown), for the focused Gaussian beam (Left), and the focused vortex beam with $m' = 1$ (Right). (color online)

results of the previous section, the noise is not the single source of discrepancy between A_n^m and $A_{n_{th}}^m$ and as consequence between F and F_{th}, Eq. 17. The inverse filtering while very efficient does not achieve a perfect synthesis of the looked for pressure fields, Fig 10. For instance, the experimental measurements are not perfectly axisymmetric and this will have an impact on the azimuthal force. For the axial plane, (xz), OMP and ASM methods also provide quite a good reconstruction on main and secondary lobes. The "X-shape" and high pressure at the focus, features expected for sharply focused beam, are perfectly reproduced, while the Lebedev quadrature estimation has some spurious amplitude oscillations. These oscillations have a comparable period with the one observed on the axial force, F_z, Fig. 7, in the numerical simulation when noise was present. We provided an explanation for this phenomenon in the previous section. As a result, both the OMP and ASM are able to estimate the incident BSC A_n^m and hence the acoustic pressure field in the volume of interest around the focus.

Finally, we use these obtained BSC of the focused Gaussian beam and the vortex beam $m' = 1$ to calculate the radiation forces exerted on polystyrene spheres of radius $r = 0.1\lambda$ with Eq. 1, 2, 3. The results are shown on Fig. 11 and Fig. 12. The axial force obtained with Lebedev method is not presented on the Figures since it's very fluctuating like its reconstruction on (xz) plane. As in the previous section, the relative error of the experimental forces for Gaussian beam and vortex are calculated and reported in tables Tab.III, IV.

Relative error	Lebedev	OMP	ASM
F_ρ	0.036	0.036	0.012
F_z	0.23	0.11	0.07

TABLE III. Relative error of the experimental forces for three methods (Gaussian beam)

According to Fig. 11, for a focused Gaussian beam and for each method the radial force is in good agreement with the theoretical one. Theoretically no azimuthal force is applied, but a weak rotational force exists in the force estimation by three methods. This dissimilarity of azimuthal force can be due to the difference between the theoretical and experimental field synthesised by inverse filtering, as well as the presence of the noise in the measurements. As

Relative error	Lebedev	OMP	ASM
F_ρ	0.027	0.057	0.034
F_ϕ	0.71	0.6	0.99
F_z	0.8	0.14	0.14

TABLE IV. Relative error of the experimental forces for three methods (Acoustic vortex $m' = 1$)

for the axial force, the force estimated by ASM is very close to the theoretical one with a very low relative error of 0.07. However, the one calculated by OMP appears to be oscillating though in the reconstruction on plane (xz) no oscillations are visible. Note that the trap slope is positive for both radial and axial forces. Therefore at the origin the force is null but the equilibrium is unstable. To achieve acoustical tweezers for a stiffer and denser particle compared to water, cancellation of the pressure field at the focus is required as the case studied below.

For the focused vortex beam of charge $m' = 1$, the forces are quite similar with the ones obtained by adding noise in the numerical assessment of the three methods (see previous section). First, the computation of the radial force agrees with the theoretical force whatever the method. Secondly, the azimuthal forces computed by the experimental BSC are different from the theoretical one. These differences are caused by the value of A_n^m coefficients outside column $m = 1$. If we keep only column $m = 1$ and recalculate the azimuthal force, then, all the forces for different methods superpose with the theoretical force. This filtering makes the pressure modulus axisymmetric and eliminates any anisotropy in the transverse plane whatever its origin inverse filtering imperfection or biased estimation of BSC. The third observation is that both OMP and ASM provide a good estimate of the axial force which has the same negative slope as the theoretical one, i.e same trap strength and stiffness. The OMP axial force has some fluctuations, but performs much better than the Lebedev method, the force obtained with ASM is smooth and close to the theory but with a shift about 0.2λ of the equilibrium position where $F_z = 0$. This shift can be caused by a slight shift 0.2λ ($0.25mm$) of the focal point in the experimental measurements. As reported in the Tab. IV, even with this shift, the relative error is small (0.14), by cancelling the shift, the relative errors will decrease to 0.091 and 0.085 for the OMP and ASM respectively which are very similar to the numerical estimations in the Tab. II of section III.

V. CONCLUSION

In this paper, the measurement of the radiation pressure on an elastic sphere exerted by acoustic tweezers is presented. The radiation force is not measured directly but is obtained from measurements of the pressure field associated with a model (see Eqs.1-3). To obtain the forces, it is necessary to estimate the BSC from experimental sampling of the pressure field. Three methods were developed in section III: the Lebedev double layer sphere quadrature, the OMP method, and the ASM. First, we assessed the methods by simulating an acoustic vortex of charge $m' = 1$ with 5% noise. The results show that all these methods can recover the BSC. In spite of that, the forces computed by the different methods agree well with the theory, except the Lebedev quadrature for which the axial force is fluctuating.

The experimental verification of these methods is done in section IV. Compared with the

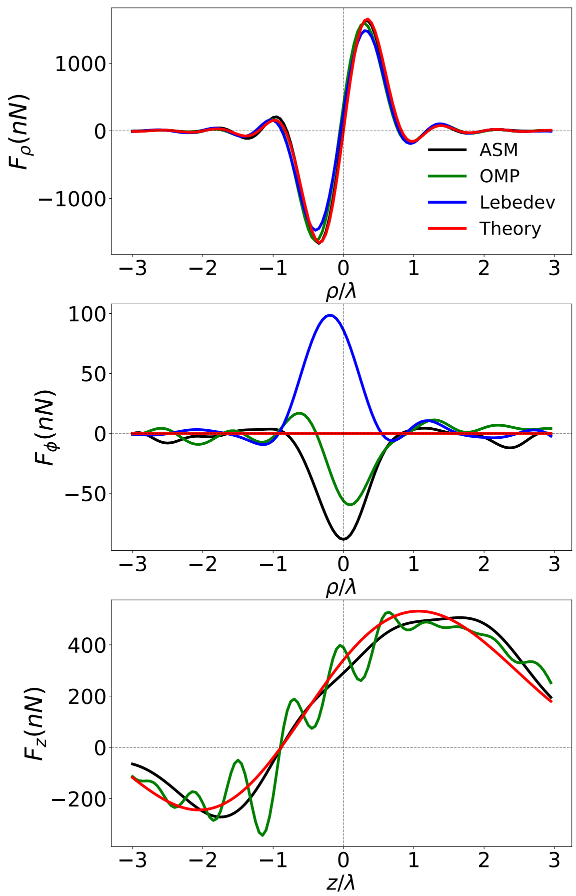

FIG. 11. Experimental radial F_ρ, azimuthal F_ϕ and axial F_z forces exerted on an polystyrene sphere of radius $r = 0.1\lambda$ in a focused Gaussian beam with charge $m' = 0$. (color online)

measurements in (xy) plane, the reconstructions of the field by the three methods are similar and almost identical. Nevertheless, for (xz) plane reconstructions, the field rebuilt by the Lebedev quadrature contains a lot of oscillations. Apart from that, both the OMP method and the angular spectrum method are in good agreement with the experimental data. From the analysis of the forces, the OMP and angular spectrum (ASM) methods allow to predict the radial and axial forces with a good precision and the azimuthal force with a lower

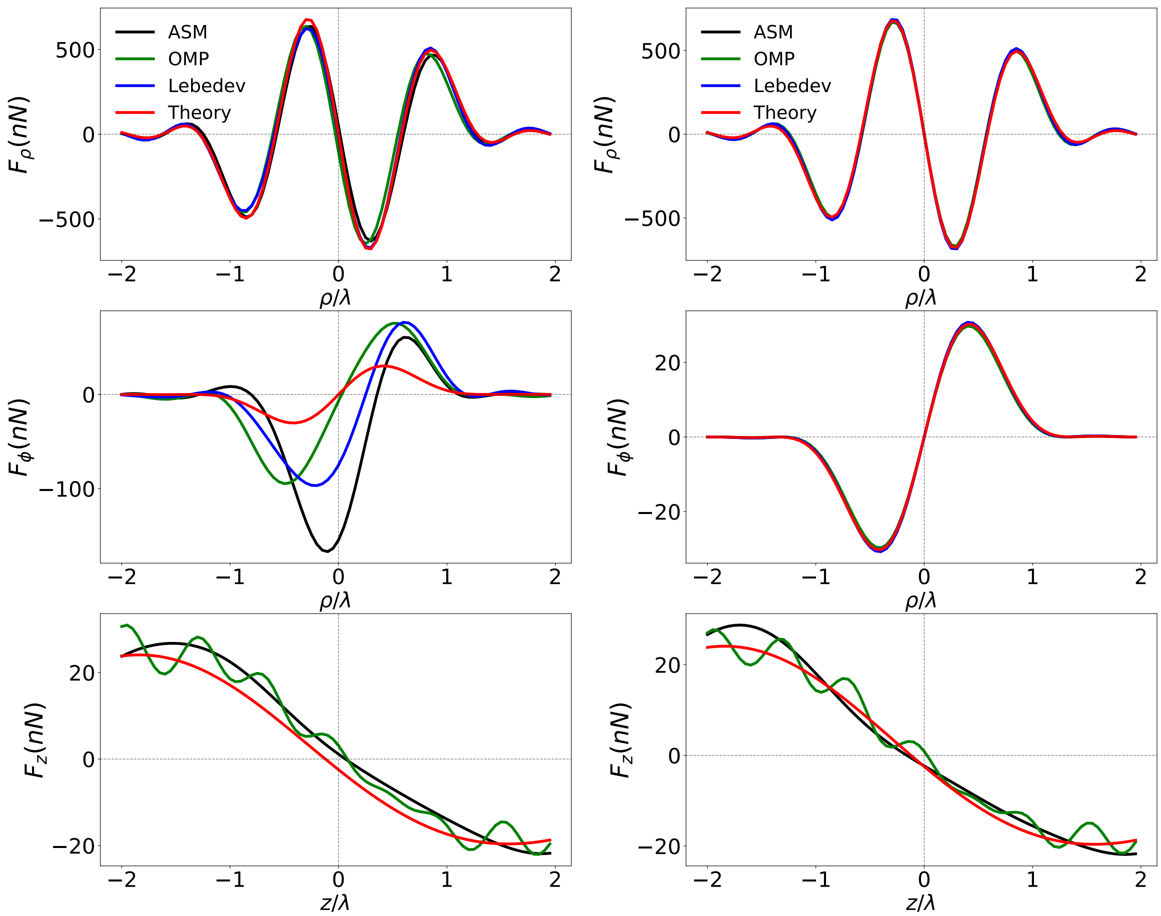

FIG. 12. Experimental radial F_ρ, azimuthal F_ϕ, axial F_z forces exerted on an polystyrene sphere of radius $r = 0.1\lambda$ in a focused vortex beam with charge $m' = 1$, calculated by the total coefficents (Left), and only by the BSC in column $m = 1$ (Right). (color online)

precision because it is sensitive to the noise outside column $m' = 1$ of the matrix of the BSC.

With the help of these methods, we are able to anticipate the radiation forces by measuring the acoustic field. As presented in previous sections, a very important component of three dimensional radiation force is the axial force which is much smaller than the transverse ones. In our experiments, we were capable to measure the axial force with a low relative error of 0.14. For further measurements, this accuracy can be improved by increasing the axial force, for example, in the case of an acoustic vortex we can increase the aperture angle α_0 (Fig.1) to get larger axial forces. At the same time, reducing the noise by any methods: shielding, averaging, filtering would help. The SNR leading to spurrious standing wave is the main limitation for axial or azimuthal force measurements.

ACKNOWLEDGMENTS

This work was supported by French state funds managed by the ANR within the Investissements d'Avenir programme under reference ANR-11-IDEX-0004-02, and more specifically within the framework of the Cluster of Excellence MATISSE led by Sorbonne Universités.

VI. REFERENCE

REFERENCES

[1] A. Ashkin. Acceleration and trapping of particles by radiation pressure. *Phys. Rev. lett.*, 24(4):156, 1970.

[2] A. Ashkin, J. M. Dziedzic, J.E. Bjorkholm, and S. Chu. Observation of a single-beam gradient force optical trap for dielectric particles. *Opt. lett.*, 11(5):288–290, 1986.

[3] A. Ashkin, J. M. Dziedzic, and T. Yamane. Optical trapping and manipulation of single cells using infrared laser beams. *Nature*, 330(6150):769, 1987.

[4]D. Baresch. *Acoustic tweezers: trapping and manipulation of an object by radiation pressure of a progressive wave.* PhD thesis, Université Pierre et Marie Curie-Paris, Paris 6, 2014.

[5]D. Baresch, J-L. Thomas, and R. Marchiano. Spherical vortex beams of high radial degree for enhanced single-beam tweezers. *J. Appl. Phys.*, 113:184901, 2013.

[6]D. Baresch, J-L. Thomas, and R. Marchiano. Three-dimensional acoustic radiation force on an arbitrarily located elastic sphere. *J. Acoust. Soc. Am.*, 133(1):25–36, 2013.

[7]D. Baresch, J-L. Thomas, and R. Marchiano. Observation of a single-beam gradient force acoustical trap for elastic particles: acoustical tweezers. *Phys. Rev. lett.*, 116(2):024301, 2016.

[8]D. Baresch, J-L. Thomas, and R. Marchiano. Orbital angular momentum transfer to stably trapped elastic particles in acoustical vortex beams. *Phys. Rev. lett.*, 121(07):074301, 2018.

[9]M. Baudoin, J-C. Gerbedoen, A. Riaud, O. Bou Matar, N. Smagin, and J-L. Thomas. Folding a focalized acoustical vortex on a flat holographic transducer: Miniaturized selective acoustical tweezers. *Sci. Adv.*, 5:eaav1967, 2019.

[10]Casper H. L. Beentjes. Quadrature on a spherical surface. *Working note available on the website http://people. maths. ox. ac. uk/beentjes/Essays*, 2015.

[11]T. T. Cai and L. Wang. Orthogonal matching pursuit for sparse signal recovery with noise. *IEEE T. Inform. Theory*, 57(7):4680–4688, 2011.

[12]A. R. Carter, Y. Seol, and T. T. Perkins. Precision surface-coupled optical-trapping assay with one-basepair resolution. *Biophys. J.*, 96(7):2926–2934, 2009.

[13]D. J. Collins, C. Devendran, Z.C. Ma, J.W. Ng, A. Neild, and Y. Ai. Acoustic tweezers via sub–time-of-flight regime surface acoustic waves. *Sci. Adv.*, 2(7):e1600089, 2016.

[14]X.Y. Ding, Sz-Chin S. Lin, B. Kiraly, H.J. Yue, S.X. Li, I-K. Chiang, J.J. Shi, S. J Benkovic, and T. J. Huang. On-chip manipulation of single microparticles, cells, and organisms using surface acoustic waves. *P. Natl. Acad. Sci. USA*, 109(28):11105–11109, 2012.

[15]Y. C. Eldar, P. Kuppinger, and H. Bolcskei. Block-sparse signals: Uncertainty relations and efficient recovery. *IEEE T. Signal Proces.*, 58(6):3042–3054, 2010.

[16]H. Goldstein, C. P. Poole, and J. L. Safko. *Classical Mechanics (3rd ed.)*. Addison-Wesley, 2001.

[17]Silva G.T., Lopes J.H., and Mitri F. G. Off-axial acoustic radiation force of repulsor and tractor bessel beams on a sphere. *IEEE T. Ultrason. Ferr.*, 60(6):1207–1212, 2013.

[18]Silva G.T., Lobo T.P., and Mitri F.G. Radiation torque produced by an arbitrary acoustic wave. *EPL*, 97:54003, 2012.

[19]B. T. Hefner and P. L. Marston. An acoustical helicoidal wave transducer with applications for the alignment of ultrasonic and underwater systems. *J. Acoust. Soc. Am.*, 106(6):3313–3316, 1999.

[20]L. V. King. On the acoustic radiation pressure on spheres. *P. Roy. Soc. Lond. A Mat.*, 147(861):212–240, 1934.

[21]V. I. Lebedev and D. N. Laikov. A quadrature formula for the sphere of the 131st algebraic order of accuracy. In *Doklady Mathematics*, volume 59, pages 477–481. Pleiades Publishing, Ltd.(,), 1999.

[22] J. Lee, C.Y. Lee, and K. K. Shung. Calibration of sound forces in acoustic traps. *IEEE T. Ultrason. Ferr.*, 57(10):2305–2310, 2010.

[23] T. Lionnet, s. Joubaud, R. Lavery, D. Bensimon, and V. Croquette. Wringing out dna. *Phys. Rev. lett.*, 96(17):178102, 2006.

[24] A. H. Mack, D. J. Schlingman, L. Regan, and S. G. J. Mochrie. Practical axial optical trapping. *Rev. Sci. Instrum.*, 83(10):103106, 2012.

[25] N. Malagnino, G. Pesce, A. Sasso, and E. Arimondo. Measurements of trapping efficiency and stiffness in optical tweezers. *Opt. Commun.*, 214(1-6):15–24, 2002.

[26] R. Marchiano and J-L. Thomas. Synthesis and analysis of linear and nonlinear acoustical vortices. *Phys. Rev. E*, 71(6):066616, 2005.

[27] R. Marchiano and J-L. Thomas. Doing arithmetic with nonlinear acoustic vortices. *Phys. Rev. lett.*, 101(6):064301, 2008.

[28] A. Marzo, S. A. Seah, B. W. Drinkwater, D. R. Sahoo, B. Long, and S. Subramanian. Holographic acoustic elements for manipulation of levitated objects. *Nature comm.*, 6:8661, 2015.

[29] B. Rafaely. The spherical-shell microphone array. *IEEE T. Audio Speech*, 16(4):740–747, 2008.

[30] O. A. Sapozhnikov and M. R. Bailey. Radiation force of an arbitrary acoustic beam on an elastic sphere in a fluid. *J. Acoust. Soc. Am.*, 133(2):661–676, 2013.

[31] S. L. Sobolev. Cubature formulas on the sphere invariant under finite groups of rotations. In *Selected Works of SL Sobolev*, pages 461–466. Springer, 2006.

[32]T. Strick, J-F. Allemand, D. Bensimon, and V. Croquette. Twisting and stretching single dna molecules. *Prog. Biophys. Mol. Bio.*, 74(1-2):115–140, 2000.

[33]J-L. Thomas and R. Marchiano. Pseudo angular momentum and topological charge conservation for nonlinear acoustical vortices. *Phys. Rev. lett.*, 91(24):244302, 2003.

[34]J. Wu. Acoustical tweezers. *J. Acoust. Soc. Am.*, 89(5):2140–2143, 1991.

[35]W.J. Xie, C.D. Cao, Y.J. Lü, Z.Y. Hong, and B. Wei. Acoustic method for levitation of small living animals. *Appl. Phys. Lett.*, 89(21):214102, 2006.